Corrosion Science 51 (2009) 833–840

Contents lists available at ScienceDirect

Corrosion Science

journal homepage: www.elsevier.com/locate/corsci

Corrosion behaviour in alkaline medium of zinc phosphate coated steel obtained by cathodic electrochemical treatment

Florica Simescu, Hassane Idrissi *

Laboratoire MATEIS UMR CNRS 5510, Equipe RI2S, INSA – Lyon, Bât. L. Vinci, 21 Av. Jean Capelle, 69621 Villeurbanne Cedex, France

ARTICLE INFO

Article history:
Received 21 October 2008
Accepted 19 January 2009
Available online 23 February 2009

Keywords:
A. Mild steel
B. EIS
C. Alkaline corrosion

ABSTRACT

The present work evaluated the ability of zinc phosphate coating, obtained by cathodic electrochemical treatment, to protect mild steel rebar against the localized attack generated by chloride ions in alkaline medium. The corrosion behaviour of coated steel was assessed by open circuit potential, potentiodynamic polarization and electrochemical impedance spectroscopy. The chemical composition and the morphology of the coated surfaces were evaluated by X-ray diffraction and scanning electron microscopy. Cathodically phosphated mild steel rebar have been studied in alkaline solution with and without chloride simulating the concrete pore solution. For these conditions, the results showed that the slow dissolution of the coating generates the formation of calcium hydroxyzincate ($Ca(Zn(OH)_3)_2{\cdot}2H_2O$). After a long immersion time in alkaline solution with and without Cl^-, the coating is dense and provides an effective corrosion resistance compared to mild steel rebar.

1. Introduction

Steel in concrete structures is normally protected from corrosion by passive film due to the alkalinity of the concrete. However, in presence of water and oxygen with a sufficient amount of chloride and/or carbon dioxide, this film can be destroyed and corrosion occurs. The corrosion products cause structures damages as cracks, accelerating the corrosion process. The influence of the Cl^- ions in depassivating the steel surface even at high pH levels can be seen as a function of the net balance between two competing processes: stabilization (and repair) of the film by OH^- ions and damage of the film by Cl^- ions [1].

For this reason, many studies have been performed to find out the best method of preventing corrosion in reinforcing bars [2,3]. Among the possible anti-corrosion methods, phosphated reinforcing bars are employed to extend the life-time of the rebars in concrete structures [2,4]. The literature shows that the alkaline stability of phosphate coatings depends on their chemical composition and their crystal structure [5]. These phosphate coatings [6] are generally composed of hopeite ($Zn_3(PO_4)_2{\cdot}4H_2O$ and phosphophyllite ($Zn_2Fe(PO_4)_2{\cdot}4H_2O$). The alkaline solubility of hopeite is higher than that of phosphophyllite [7–10]. Thus, the alkaline solution dissolves firstly the coating composed of hopeite. Then, the dissolution reaction continues with the layers rich in iron and mainly composed of phosphophyllite [11].

There are few published fundamental studies concerning the alkaline stability of the phosphate coating and particularly in Ca^{2+} saturated solution.

The aim of this work is to develop zinc phosphate coatings on reinforcing bars to study its stability and corrosion behaviour in an alkaline solution. Synthetic media, saturated in Ca^{2+} ions, were used to simulate the aqueous solution existing in concrete pores at early stages and chloride ions were added to simulate degraded concrete. These tests in simulated concrete pore solutions are necessary to understand the protection ability of the phosphate coating, prior to its use on reinforcing bars embedded in concrete.

2. Experimental

2.1. Substrate and coating

Experiments are realized on mild steel bars (with 0.2 wt.% C, and with a diameter of 8 mm), noted MS. The phosphated surface (noted PMS) is approximated as a cylinder with a length of 2 cm corresponding to a surface of 5.5 cm^2. Surfaces are chemically pickled with 36.5% HCl during one minute, and then rinsed several times with deionized water. After rinsing, samples are immersed in the phosphating bath. Cathodic electrochemical treatment (noted CET) is performed at an applied potential of −1800 mV vs saturated calomel electrode (SCE), for 10 min at room temperature. The bath composition is given in Table 1. After the cathodic phosphating process, the samples are rinsed with deionised water and dried in ambient air.

* Corresponding author. Tel.: +33 (0) 472 43 89 20; fax: +33 (0) 472 43 87 15.
E-mail address: Hassane.Idrissi@insa-lyon.fr (H. Idrissi).

0010-938X/$ - see front matter © 2009 Elsevier Ltd. All rights reserved.
doi:10.1016/j.corsci.2009.01.010

Table 1
Composition and pH of the phosphating bath.

Composition	pH
Zn^{2+} (0.17 M) + PO_4^{3-} (0.34 M) + Ni^{2+} (0.005 M) +NO_3^- (0.08 M)	2.1

Table 2
Description of the various electrolytes used.

Solution	$Ca(OH)_2$ (mol/L)	NaOH (mol/L)	KOH (mol/L)	NaCl (g/L)	pH
S	Saturation	0.001	0.001	0	12.6
SC	Saturation	0.001	0.001	35	12.5

2.2. Electrolytes

The PMS and MS samples were immersed in alkaline solutions simulating the concrete interstitial electrolyte at ambient temperature (Table 2). A saturated calcium hydroxide solution (noted S) has been used to simulate the aqueous alkaline content of the concrete pore solutions, with an approximate pH of 12.6. To simulate the aqueous phase of a concrete contaminated with chloride, 35 g/L NaCl was introduced in the S solution to obtain an electrolyte designated by SC. The pH of the solution containing chloride was 12.5.

2.3. Electrochemical measurements

Different electrochemical techniques were used to evaluate the corrosion behaviour of the PMS and MS samples: open circuit potential (noted E_{corr}), potentiodynamic polarization and electrochemical impedance spectroscopy (EIS) measurements. E_{corr} was monitored during 8 days. Polarization curves ($I = f(E)$) were plotted with a scan rate of 0.1 mV/s from −100 to 1000 mV vs E_{corr} in the anodic direction. EIS measurements were carried out at corrosion potential with a frequency variation between 100 kHz and 0.01 Hz and a potential sine signal of 10 mV. Impedance data were fitted using ZImp software.

2.4. Surface analysis

The morphology and the coating compositions were studied by scanning electron microscopy (SEM) in secondary electron imaging (SEI) and energy dispersive X-ray spectroscopy (EDS) modes. Coating crystallographic structure was analyzed by X-ray diffraction measurement (XRD) using $Cu_{K-L(2,3)}$ radiation. The phases formed where identified from the peaks obtained by XRD analyses, this identification being founded on the elements determined by EDX analyses.

3. Results and discussion

3.1. Morphology and composition of the coating

The SEM observations show that the coating is compact, well crystallized and covers completely the steel surface (Fig. 1a). The structure is, in a few small areas, characterized by nodules (diameter around 1 μm, Fig. 1b) and majorities of sand roses (Fig. 1c), which have lamellar shapes with higher sizes (up to 30 μm, Fig. 1d). The nodules are uniformly mixed with the sand roses. They also present many pores formed by the dihydrogen bubbles released during the coating elaboration. The thickness of the phosphate coating obtained by this treatment is ∼30 μm. By EDS analysis, the coating composition exhibits 43 wt.% of zinc and 20 wt.% of phosphorus (Table 3).

X-ray diffraction measurement performed on this steel coated indicates the presence of three phases: hopeite ($Zn_3(PO_4)_2{\cdot}4H_2O$), phosphophyllite ($Zn_2Fe(PO_4)_2{\cdot}4H_2O$) and metallic zinc (Fig. 2). According to Kouisni et al. [12], these phosphate coatings contain only "hopeite" phase. Indeed, at the imposed potential, the phos-

Table 3
PMS composition.

Elements (wt.%)	O	P	Fe	Zn
PMS composition	34.3 ± 1.0	20.4 ± 1.0	2.3 ± 1.0	43 ± 1.0

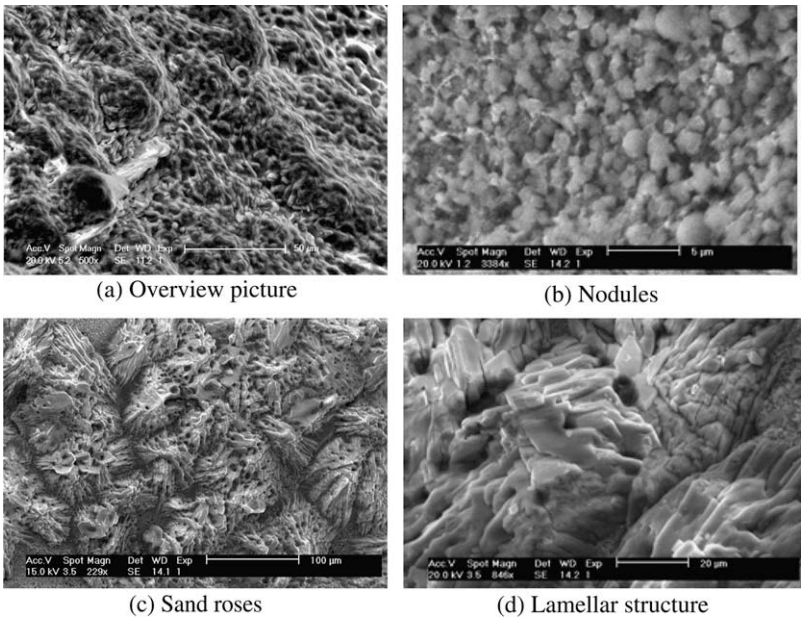

Fig. 1. SEM micrographs of mild steel coated surface: (a) overview picture, (b) nodules, (c) sand roses and (d) lamellar structure.

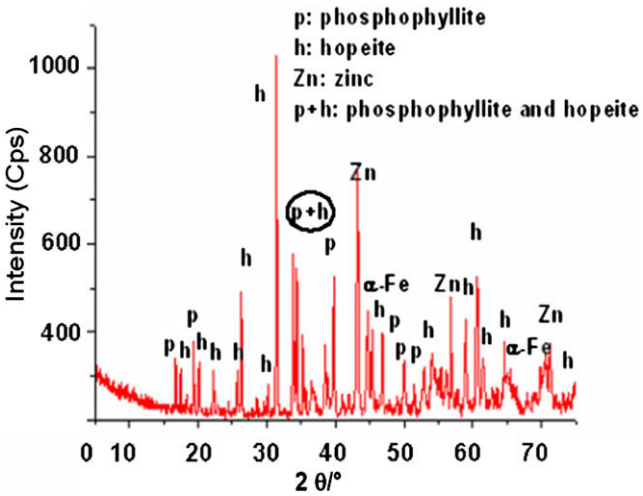

Fig. 2. X-ray pattern of PMS.

phophyllite formation may not take place [13]. But, the presence of phosphophyllite phase is related to the MS dissolution in the acid bath (pH = 2.2) before applying the potential [14]. According to this, the possible reactions for cathodic electrochemical treatment are:

– hopeite and phosphophyllite formation

$$3Zn^{2+} + 2H_2PO_4^- + 4H_2O \rightarrow Zn_3(PO_4)_2 \cdot 4H_2O + 4H^+ \quad (1)$$

$$2Zn^{2+} + Fe^{2+} + 2H_2PO_4^- + 4H_2O \rightarrow Zn_2Fe(PO_4)_2 \cdot 4H_2O + 4H^+; \quad (2)$$

– the zinc deposition and the hydrogen evolution

$$Zn^{2+} + 2e^- \rightarrow Zn \quad (3)$$

$$2H^+ + 2e^- \rightarrow H_2\uparrow . \quad (4)$$

3.2. Corrosion behaviour

3.2.1. Alkaline medium (pH = 12.6)

3.2.1.1. Corrosion potential evolution. The E_{corr} monitoring, for PMS and MS, shows a trend to higher values than those recorded at the immersion. For the MS sample (Fig. 3a), the corrosion potential after passivation is around −250/−300 mV/SCE. Thus, after 3 days

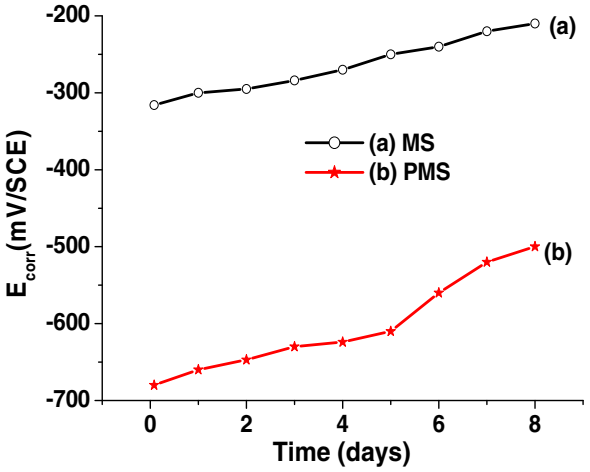

Fig. 3. E_{corr} evolution for (a) MS and (b) PMS in S solution.

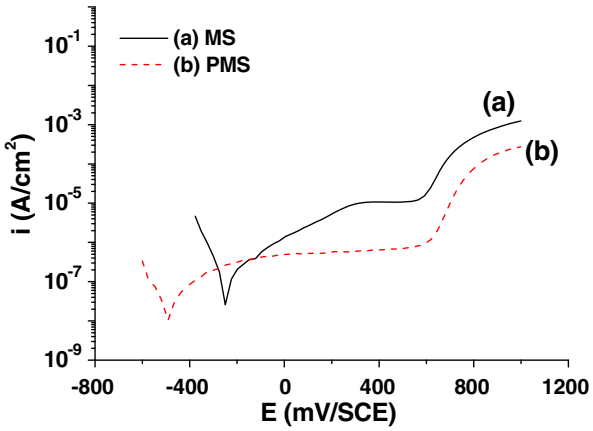

Fig. 4. Polarization curves for MS and PMS after 8 days of immersion in S solution.

of immersion in S solution, the E_{corr} is stabilized in the passive region during all the test period. For the coated steel, more cathodic potential values are observed with an increase up to −500 mV/SCE, after 8 days of immersion. A similar behaviour is reported by Andrade et al. [15] for steel rebars and by Belaid et al. [16] for galvanized reinforcing steel at the same pH value.

Zinc is an amphoteric metal, stable over a wide range of pH (6–12.5). At a pH above 12.5, zinc dissolution and hydrogen evolution produce a continuous dissolution of the metal. This is possible because the nodules are uniformly mixed with the sand roses and this distribution gives for PMS sample a similar behaviour to that of galvanized steel.

However, in the concrete interstitial electrolyte, the presence of Ca^{2+} induces further passivation of the metal surface. In these conditions, a slow dissolution of the metallic zinc presented in this coating is observed.

3.2.1.2. Polarization curves. Fig. 4 shows the polarization curves of PMS and MS specimens after 8 days of immersion in S solution. It is shown that an extended passive region exists on the anodic polarization part for the uncontaminated chloride solution. This region starts immediately after E_{corr} and continues up to the pitting potential (E_{pit}) at 560 mV/SCE (for MS specimen) and ~600 mV/SCE (for PMS specimen). PMS exhibits lower passive current density, ~0.3 μA/cm² than MS, ~8 μA/cm² (Table 4). PMS presents a lower current density that MS which can be related to the different nature of the passive layer, as zinc phosphate coating is present on the surface.

As obtained from the corrosion potential measurements (Fig. 3), the E_{corr} of the PMS electrode (−500 mV/SCE) is more negative that of the MS electrode (−240 mV/SCE). The phosphate coating is a mixture of hopeite, phosphophyllite and zinc, the presence of zinc conferring to the PMS electrode a similar behaviour with that of galvanized reinforcing steel at the same pH value.

It can be concluded that PMS in Ca^{2+} saturated solution presents higher stability than MS and that zinc phosphate coating offers an extra corrosion resistance to MS after 8 days of immersion.

Table 4
Corrosion potential, current density (at corrosion potential) and pitting potential for MS and PMS specimens after 8 days of immersion in S solution.

Sample	E_{corr} (mV/SCE)	i (μA/cm²)	E_{pit} (mV/ECS)
MS	−240	8	560
PMS	−500	0.3	600

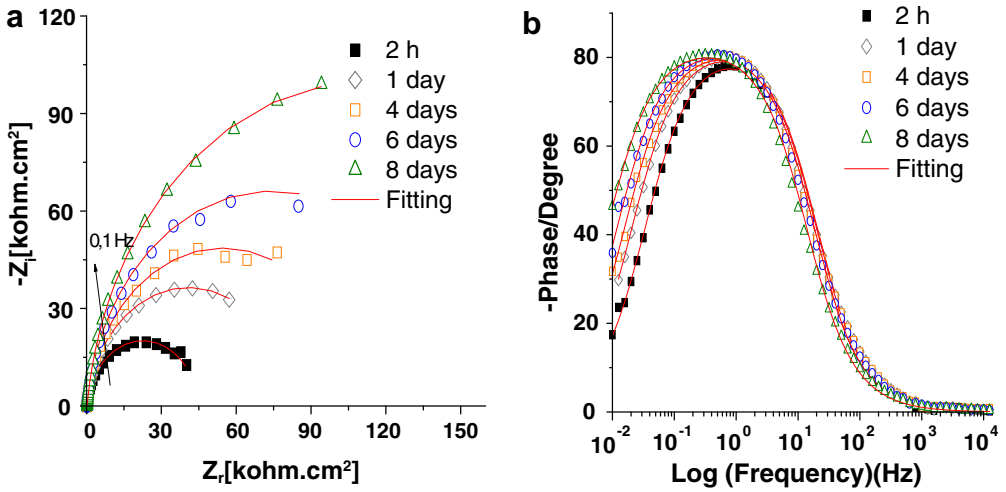

Fig. 5. (a) Nyquist diagram and (b) Bode diagram of MS from 2 h to 8 days of immersion in S solution (experimental values (dots) and fitted values (full line)).

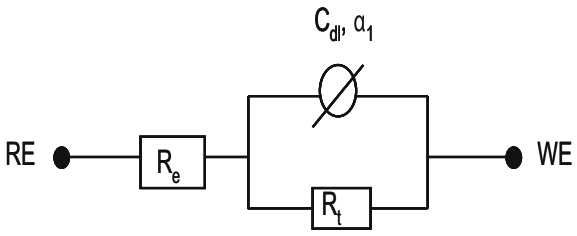

Fig. 6. Equivalent circuit used for modelling the EIS data.

3.2.1.3. EIS measurements. The electrochemical impedance diagrams obtained at corrosion potential were carried out after 2 h, 1 day, 4, 6 and 8 days of immersion. For non-treated-steel, the Nyquist plots and the Bode diagrams are presented in Fig. 5a and b. A proposed R(QR) electric equivalent circuit is given in Fig. 6 where $R_e \sim 190\ \Omega\ cm^2$ corresponds to the electrolyte resistance, while C_{dl} and R_t present the double layer capacitance and the charge transfer resistance of the steel/solution interface. The electrical parameters (C_{dl},R_t) obtained through fitting EIS data, using the electric equivalent circuit R(QR), are listed in Table 5.

Table 5
Electrical parameters for MS immersed in S solution obtained through fitting EIS data.

Time (day)	R_t (kΩ cm^2)	α	C_{dl} (μF/cm^2)	χ^2 (error factor)
0.08	44.5	0.93	66.9	5×10^{-3}
1	81.5	0.93	57.7	1×10^{-3}
4	109	0.93	55.2	1×10^{-3}
6	142	0.93	53.3	8×10^{-3}
8	223	0.93	50.6	2×10^{-3}

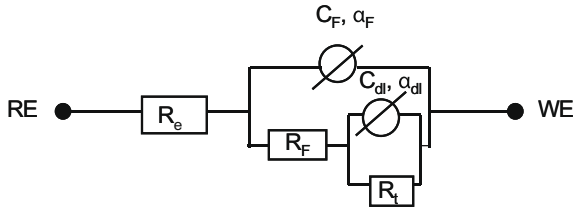

Fig. 8. Equivalent circuit used for modelling the EIS data of PMS.

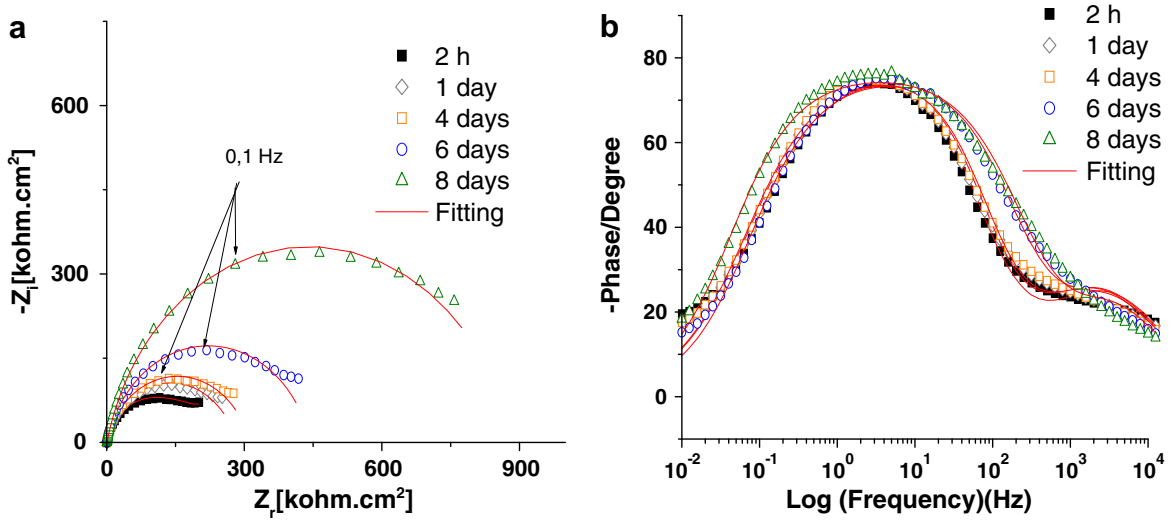

Fig. 7. Nyquist (a) and Bode (b) diagrams of PMS from 2 h to 8 days of immersion in S solution (experimental values (dots) and fitted values (full line)).

Table 6
Electrical parameters for PMS immersed in S solution obtained through fitting EIS data.

Time (day)	R_F (Ω cm^2)	α_F	C_F (μF/cm^2)	R_t (kΩ cm^2)	α_{dl}	C_{dl} (μF/cm^2)	χ^2 (error factor)
0.08	493	0.73	0.21	188	0.92	3.4	1.8×10^{-3}
1	567	0.72	0.21	313	0.93	2.11	4.3×10^{-3}
4	496	0.77	0.19	412	0.89	1.17	3.9×10^{-3}
6	500	0.71	0.15	712	0.82	0.94	2.2×10^{-3}
8	440	0.82	0.16	883	0.86	0.76	4×10^{-3}

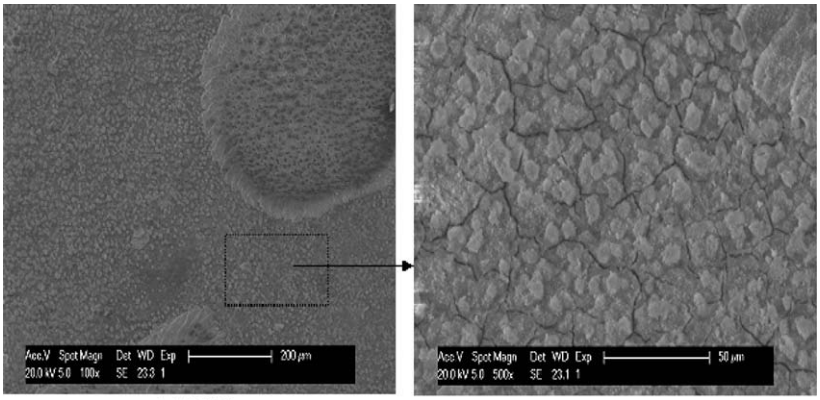

Fig. 9. SEM micrographs for PMS after 8 immersion days in S solution.

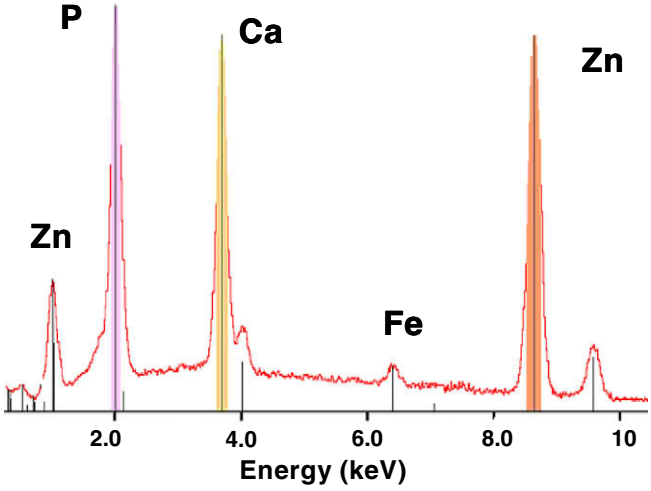

Fig. 10. EDS composition of PMS after 8 days of immersion in S medium.

These representations show one capacitive loop with a diameter increasing with the time of immersion. Thus, R_t increases simultaneously with the decrease of C_{dl}. These evolutions characterized the increase of charge transfer blocking at the steel surface and the decrease of the active area that is related to the passive film formation.

Fig. 7a and b show the Nyquist plot and Bode diagram of coated steel. Quantitative analysis of the EIS data was conducted by proposing an electric equivalent circuit where each element is representative of physical processes at the PMS surface. The proposed electric equivalent circuit is given in Fig. 8 where C_F and R_F represent the capacitance and resistance of the phosphate coating.

The Bode representations show two time constants (one at high frequency HF and another at low frequency LF) for coated steel, and thus the capacitive loop observed in the Nyquist plots is consisted of two non-decoupled capacitive loops. From these diagrams low values of C_F and C_{dl} are recorded (Table 6). The double layer

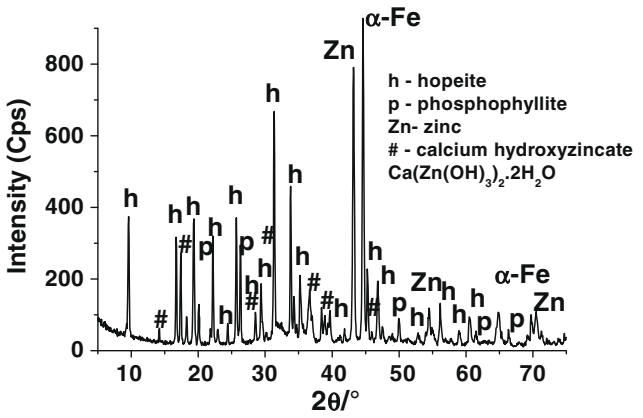

Fig. 11. X-ray pattern of coated steel after 8 days of immersion in S medium.

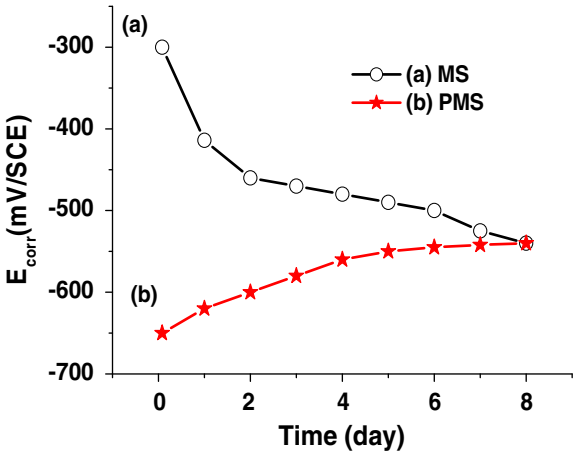

Fig. 12. E_{corr} evolution for (a) MS and (b) PMS in SC medium.

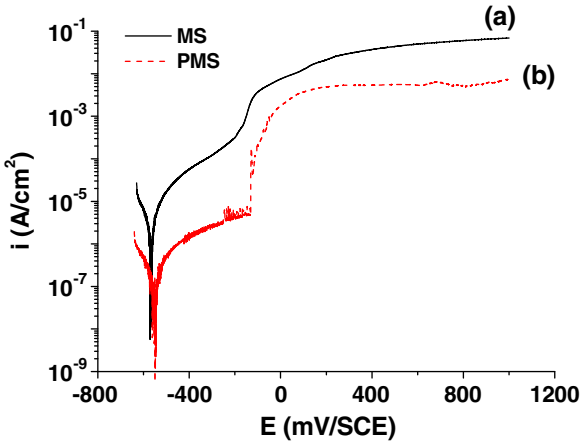

Fig. 13. Polarization curves for MS and PMS after 8 days of immersion in SC solution.

Table 7
Corrosion potential, current density (at corrosion potential) and pitting potential for MS and PMS specimens after 8 days of immersion in SC solution.

Sample	E_{corr} (mV/SCE)	i (μA/cm²)	E_{pit} (mV/SCE)
MS	−570	20	−180
PMS	−550	0.6	−120

capacitance $C_{dl} < 2.5$ μF/cm² shows that a small part R_t of the coated steel surface is involved in the electrochemical reactions at steel/solution interface [17–21]. The corrosion reaction occurs only on a very small fraction of the total coated steel area. These results indicate that this coating provides efficient protection of steel at pH 12.6 (in S solution).

SEM micrographs (Fig. 9) and surface analysis (EDS and XRD) on the coated steel, after 8 immersion days at pH 12.6, reveal a different morphology for this protective coating.

The crystals size (sand roses and nodules) decreases considerably during 8 immersion days at pH 12.6. EDS analysis shows that this coating is composed of P, Ca, Zn and Fe (Fig. 10).

The XRD analysis (Fig. 11) confirmed the presence of calcium and peaks associated with phosphate coating are also obtained.

Table 8
Electrical parameters for MS and PMS immersed in SC solution obtained through fitting EIS data.

Sample	Time (day)	R_F (kΩ cm²)	α_F	C_F (μF/cm²)	R_t (kΩ cm²)	α_{dl}	C_{dl} (μF/cm²)	χ^2 (error factor)
MS	1	–	–	–	7.9	0.92	60.6	4.4×10^{-3}
	4	–	–	–	3.8	0.88	60	9×10^{-3}
	8	–	–	–	3.4	0.89	62.5	6.6×10^{-3}
PMS	1	51.4	0.8	1.8	52.7	0.7	23	1.5×10^{-3}
	4	14.2	0.8	2.4	41.5	0.98	33	2×10^{-3}
	8	7.5	0.8	1.8	39	0.88	35	4×10^{-3}

New peaks related to the calcium hydroxyzincate formation ($Ca(Zn(OH)_3)_2{\cdot}2H_2O$) are detected.

Belaid et al. [16] have shown that this compound is the main corrosion product of galvanized steel in chloride contaminated concrete. The calcium hydroxyzincate was also identified during the galvanized steel corrosion [17,22].

Thus, at immersion of the PMS in alkaline solutions, in presence of Ca^{2+} ions, the precipitation of calcium hydroxyzincate (CaHZn) takes place. Sanchez [17] proposed the following mechanism to explain the formation of CaHZn crystals:

$$Zn + 2H_2O \rightarrow Zn(OH)_2 + H_2 \quad (5)$$

$$Zn(OH)_2 + H_2 + Ca(OH)_2 \rightarrow Ca(Zn(OH)_3)_2 \cdot 2H_2O. \quad (6)$$

3.2.2. Alkaline medium contaminated by chloride (SC)

3.2.2.1. Corrosion potential evolution. Fig. 12 presents the E_{corr} evolution, for PMS and MS samples, during the immersion in alkaline medium contaminated by chloride. The E_{corr} of MS decreases (Fig. 12a) and stabilizes to −550 mV/SCE after 8 days of immersion. This evolution corresponds to an active state of the steel. For the coated steel, E_{corr} increases and stabilizes after 5 days at a value similar to that measured for steel after 8 days of immersion (∼−550 mV/SCE).

Contrary evolution is obtained in time for the MS and PMS electrode because the PMS sample is first subject to a coating deterioration by the medium alkalinity, and secondly to the steel corrosion through the open pores of the coating. In comparison with the E_{corr} evolution measured in S medium (Fig. 3) PMS sample shows the same behaviour. Similar results are reported by Andrade et al. [15] and by Arenas et al. [22].

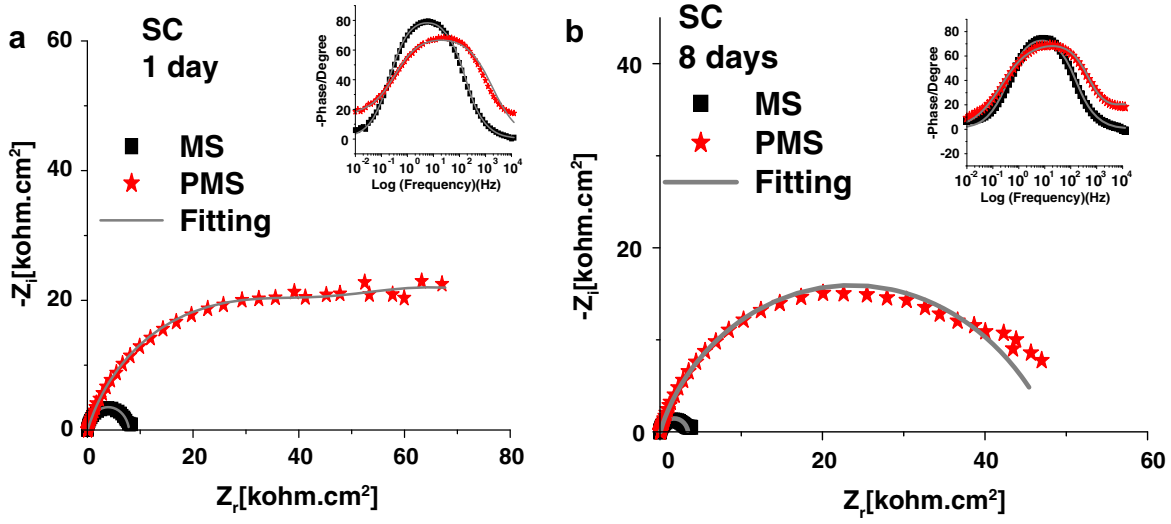

Fig. 14. Nyquit and Bode diagram of MS and PMS, experimental values (dots) and fitted values (full line), after (a) 1 day and (b) 8 days of immersion in SC solution.

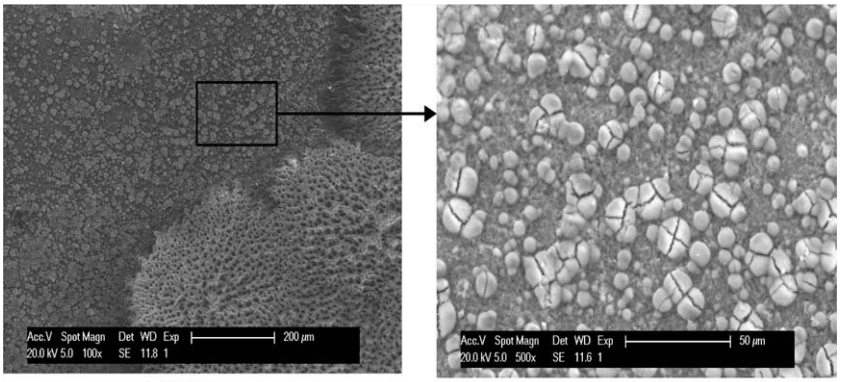

Fig. 15. SEM micrographs for PMS after 8 immersion days in SC solution.

3.2.2.2. Polarization curves. The polarization curves of both PMS and MS samples after 8 days of immersion in SC solution are presented in Fig. 13. No significant potential shift is observed between the coated and the uncoated steels. The increase of the passive current density with the modified pitting potential from 560 to −180 mV/SCE (for MS specimen) and from 600 to −120 mV/SCE (for PMS) was observed. The drop of two decades of the current density at corrosion potential of PMS with respect to the MS shows the beneficial role of the zinc phosphate coating obtained by CET. The measured current density (at corrosion potential) reaches a reproducible value of 0.6 μA/cm^2 (Table 7).

In conclusion, after 8 days of immersion in SC solution, PMS is characterized by a lower current density and a higher pitting potential. This demonstrates that the surface treatment decreases the pitting susceptibility by increasing the pitting potential in about 60 mV compared to MS.

3.2.2.3. EIS measurements. The electrochemical impedance diagrams (Nyquist and Bode) of steel and coated steel, obtained at corrosion potential after 1 day and 8 days of immersion in SC solution are presented in Fig. 14. These diagrams present one capacitive loop for steel and two non-decoupled capacitive loops for coated steel. The equivalent electrical circuit describing all detected phenomena during 8 immersion days has a one time constant for steel (Fig. 6), and two time constants for coated steel (Fig. 8). The electrical parameters obtained after modelling EIS data are listed in Table 8.

The impedance diagrams evolution (Fig. 14) with the immersion time shows that the chloride presence in SC solution gives simultaneously a competition between the formation and local destruction of the film obtained by the slow coating dissolution. This classical corrosion mechanism leads to the diminution of R_t and to the increase of the double layer capacitance C_{dl}. It can be noticed that during immersion, for PMS, the R_t value remains higher than for MS. R_F is the electrical resistance of ion transfer through the open coating pores. It decreases with time: this evolution corresponds to the electrolyte diffusion into the coating pores.

In the case of PMS, the film morphology is similar to that observed in the absence of chloride ions (Fig. 9) and the X-ray pattern shows the presence of calcium hydroxyzincate ($Ca(Zn(OH)_3)_2{\cdot}2H_2O$. Thus, the calcium hydroxyzincate formation occurs even in the presence of chloride ions (Fig. 15). Compared with the MS, the formation of this film due to the slow dissolution of the coating deposited before, leads to a better protection of the steel as it is shown by the EIS diagrams (Fig. 14).

4. Conclusion

New protective coatings have been developed by cathodic electrochemical treatment (CET) on reinforcing bars to prevent its corrosion in concrete. The coatings obtained with the cathodic phosphating process are composed of three phases: hopeite, phosphophyllite and metallic zinc. The presence of these phases (including metallic zinc) is confirmed directly by XRD analyses and by the phosphate coating behaviour in the different exposed media.

In alkaline solution with or without chloride, the phosphated mild steel sample (PMS) is more resistant than mild steel (MS) alone. Indeed, this study showed, during the first immersion days in the alkaline media (pH = 12.6) a slow dissolution of the hopeite and phosphophyllite and a strong dissolution of metal zinc. This latter, in the presence of calcium, forms a complex hydroxyzincate that is followed by the precipitation of calcium hydroxyzincate ($Ca(Zn(OH)_3)_2{\cdot}2H_2O$). Thus, a dense and protective layer is formed.

With a chloride ions solution, at very high concentrations exceeding the chloride threshold tolerated for the start of steel corrosion in alkaline media ($[Cl^-]/[OH^-] > 0.6$), the calcium hydroxyzincate film formed by this treatment contributes to the decrease of chloride aggressiveness and provides an effective protection against the corrosion of steel reinforcements.

References

[1] B. Assouli, F. Simescu, G. Debicki, H. Idrissi, Detection and identification of concrete cracking during corrosion of reinforced concrete by acoustic emission coupled to electrochemical techniques, NDT&E Int. 38 (2005) 682–689.
[2] M. Manna, I. Chakrabarti, N. Bandyopadhyay, Phosphate treatment of TMT rebar bundle to avoid early rusting: an option for single step process, Surf. Coat. Technol. 201 (2006) 1583–1588.
[3] M. Manna, N. Bandyopadhyay, D. Bhattacharjee, Effect of plating time for electroless nickel coating on rebar surface: an option for application in concrete structure, Surf. Coat. Technol. 202 (2008) 3227–3232.
[4] G. Bikulčius, O. Girčiene, V. Burokas, Corrosion behaviour in alkaline media of steel with various conversion coatings in concrete, Russ. J. Appl. Chem. 76 (2003) 1759–1763.
[5] D. Weng, P. Jokiel, A. Uebleis, H. Boehni, Corrosion and protection characteristics of zinc and manganese phosphate coatings, Surf. Coat. Technol. 88 (1996) 147–156.
[6] J. Donofrio, Zinc phosphating, Met. Finish. 98 (2000) 57–73.
[7] K. Ogle, N. Meddahi, A. Tomandl, M. Wolpers, in: Proceedings of the 1st International Surface Treatments Institute of Franche-Comté Conference Automotive Industry, France, 2003.
[8] K. Ogle, A. Tomandl, N. Meddahi, M. Wompers, The alkaline stability of phosphate coatings I: ICP atomic emission spectroelectrochemistry, Corros. Sci. 46 (2004) 979–995.
[9] A. Tomandl, M. Wolpers, K. Ogle, The alkaline stability of phosphate coatings II: in situ Raman spectroscopy, Corros. Sci. 46 (2004) 997–1011.

[10] G.Y. Li, L.Y. Niu, J.S. Lian, Z.H. Jiang, A black phosphate coating for C1008 steel, Surf. Coat. Technol. 176 (2004) 215–221.
[11] M. Shoeib, M. Farouk, F. Hanna, Influence of ethoxylate surfactants on zinc phosphate coatings, Met. Finish. 95 (1997) 62–68.
[12] L. Kouisni, M. Azzi, M. Zertoubi, F. Dalard, S. Maximovitch, Phosphate coatings on magnesium alloy AM60 part 1: study of the formation and the growth of zinc phosphate films, Surf. Coat. Technol. 185 (2004) 58–67.
[13] S. Jegannathan, T.S.N. Sankara Narayanan, K. Ravichandran, S. Rajeswari, Formation of zinc–zinc phosphate composite coatings by cathodic electrochemical treatment, Surf. Coat. Technol. 200 (2006) 4117–4126.
[14] P.K. Sinha, R. Feser, Phosphate coating on steel surfaces by an electrochemical method, Surf. Coat. Technol. 161 (2002) 158–168.
[15] C. Andrade, M. Keddam, X.R. Novoa, M.C. Perez, C.M. Rangel, H. Takenouti, Electrochemical behaviour of steel rebars in concrete: influence of environmental factors and cement chemistry, Electrochim. Acta 46 (2001) 3905–3912.
[16] F. Belaid, G. Arliguie, R. Francois, Corrosion products of galvanized rebars embedded in chloride-contaminated concrete, Corrosion 56 (2000) 960–965.
[17] M. Sanchez, M.C. Alonso, P. Cecilio, M.F. Montemor, C. Andrade, Electrochemical and analytical assessment of galvanized steel reinforcement pre-treated with Ce and La salts under alkaline media, Cement Concrete Compos. 28 (2006) 256–266.
[18] J. Creus, H. Idrissi, H. Mazzille, F. Sanchette, P. Jancquot, Corrosion behaviour of Al/Ti coating elaborated by cathodic arc PVD process onto mild steel substrate, Thin Solid Films 346 (1999) 150–154.
[19] J. Creus, H. Mazzille, H. Idrissi, Porosity evaluation of protective coatings onto steel, through electrochemical techniques, Surf. Coat. Technol. 130 (2000) 224–232.
[20] M. Mahdavian, M.M. Attar, Investigation on zinc phosphate effectiveness at different pigment volume concentrations via electrochemical impedance spectroscopy, Electrochim. Acta 50 (2005) 4645–4648.
[21] M. Hernandez, J. Genesca, J. Uruchurtu, F. Galliano, D. Ladolt, Effect of an inhibitive pigment zinc–aluminium–phosphate (ZAP) on the corrosion mechanisms of steel in waterborne coatings, Prog. Org. Coat. 56 (2006) 199–206.
[22] M.A. Arenas, C. Casado, V. Nobel-Pujol, J. Damborenea, Influence of the conversion coating on the corrosion of galvanised reinforcing steel, Cement Concrete Compos. 28 (2006) 267–275.